

Cu–Zn Alloy Formation as Unfavored State for Efficient Methanol Catalysts

Elias Frei,^{*,[a]} Abhijeet Gaur,^[b] Henning Lichtenberg,^[b] Leon Zwiener,^[a] Michael Scherzer,^[a] Frank Girgsdies,^[a] Thomas Lunkenbein,^[a] and Robert Schlögl^[a, c]

The active sites of Cu/ZnO-based catalysts, commercially applied for the hydrogenation of CO₂ or CO₂-rich synthesis gas, are still subject of current debates. Generally, the discussion is focused on the nature of the interfacial contact between Cu and ZnO, particularly whether it is rather of oxidic (Cu–ZnO) or alloying (Cu–Zn) character. We report on kinetic investigations on a Cu/ZnO:Al high performance catalyst activated at different temperatures. Incrementally increasing temperature under reductive conditions leads also to increased CuZn-alloy formation, analyzed by *in-situ* X-ray diffraction, *in-situ* X-ray absorption spectroscopy and high resolution transmission electron microscopy. The combination of the catalytic data and the complementary characterization techniques provide valuable insights on the relevant reaction sites for CH₃OH formation. Our results highlight the complexity of the interfacial contact with evidence for Cu–ZnO reaction sites and clarify the negative impact of CuZn alloy formation on the nature of the active site.

In heterogeneous catalysis, the specific state of surfaces in terms of structural and electronic saturation was already discussed in 1914 by Haber.^[1] The conceptual evolution, that not the entire available surface but dedicated “reaction sites” are responsible for the rate of formation (or conversion), dates back to the 1920s.^[2] The activation of the reactants and the selective cleavage/formation of the corresponding bonds,

prompted the necessity of a catalogue of catalytic materials.^[3] Still today, partly due to the complexity of the applied catalysts,^[4] the identification of such “active sites” is rather challenging.^[5] Metal oxide - metal interfaces, particularly between Cu and ZnO, are examples of catalysts for which the active site is a matter of debate since decades.^[6] The dynamic behavior of the Cu/ZnO composition upon changes in the environment (temperature, pressure, gas phase etc.) or as a function of time, makes this system really intriguing.^[7] The manifold character of the synergism between Cu and ZnO focusses generally on surface alloying, surface ZnO species and the interfacial contact.^[6f,8] We could recently show that this intimate metal/oxide contact is already developed during the multi-event nature of the activation process.^[9] Within this study, we report on the impact of the activation temperature on the performance of a Cu/ZnO:Al (in atom-% 69Cu/29Zn/2Al, XRF Table S1) catalyst in CH₃OH formation (8CO₂/6CO/59H₂/27He, 30 bar, 230 °C). The catalytic results are correlated with structural data provided by various *in-situ* characterization tools such as X-ray diffraction (XRD), ambient pressure X-ray absorption spectroscopy (XAS) combining near edge structure (XANES) and extended X-ray absorption fine structure (EXAFS) at the K-edges of Cu and Zn. Coupled with electron microscopy, surface titration techniques (reactive frontal chromatography, N₂O-RFC and temperature programmed desorption, H₂-TPD) and a kinetic evaluation (apparent activation energy, E_A), the consequences of the activation temperature for the number and nature of active sites are discussed. The synthesis protocol is described briefly in the supporting information (SI). An analogously prepared catalyst showed very promising catalytic results in previous studies.^[10]

Figure 1(a) shows the Cu lattice parameter a as a function of the activation temperature in an atmosphere of 20% H₂ in He. Since a CuZn-alloy (or α -brass) has the same structural environment as Cu metal, the degree of CuZn-alloy formation is only directly visible through the corresponding lattice parameter which is enlarged by Zn incorporation. Oxygen or hydrogen contributions are excluded as source of lattice expansion.^[11] The lattice parameter was determined *in-situ* (red points, as powder) in Bragg-Brentano (BB) geometry or *quasi in-situ* (black points, as pressed pellet with inert glove box transfer) for rather surface sensitive information in parallel beam (PB) geometry (details see SI, XRD part). The *in-situ* XRD data (measured at RT to distinguish alloying from thermal expansion effects) show an incremental increase in the lattice parameter as a function of the activation temperature starting at 300 °C. The PB measurements show a significant increase in a already between 250 and

[a] Dr. E. Frei, Dr. L. Zwiener, Dr. M. Scherzer, Dr. F. Girgsdies, Dr. T. Lunkenbein, Prof. Dr. R. Schlögl

Department of Inorganic Chemistry
Fritz-Haber Institut der Max-Planck Gesellschaft
Faradayweg 4–6
14195, Berlin (Germany)
E-mail: efrei@fhi-berlin.mpg.de

[b] Dr. A. Gaur, Dr. H. Lichtenberg
Karlsruher Institut für Technologie
Institute for Chemical Technology and Polymer Chemistry and
Institute of Catalysis Research and Technology
Engesserstr. 20
76131 Karlsruhe (Germany)

[c] Prof. Dr. R. Schlögl
Department of Heterogeneous Reactions
Max-Planck-Institute for Chemical Energy Conversion
Stiftstrasse 34–36
45470 Mülheim an der Ruhr (Germany)

 Supporting information for this article is available on the WWW under <https://doi.org/10.1002/cctc.202000777>

 © 2020 The Authors. Published by Wiley-VCH Verlag GmbH & Co. KGaA. This is an open access article under the terms of the Creative Commons Attribution License, which permits use, distribution and reproduction in any medium, provided the original work is properly cited.

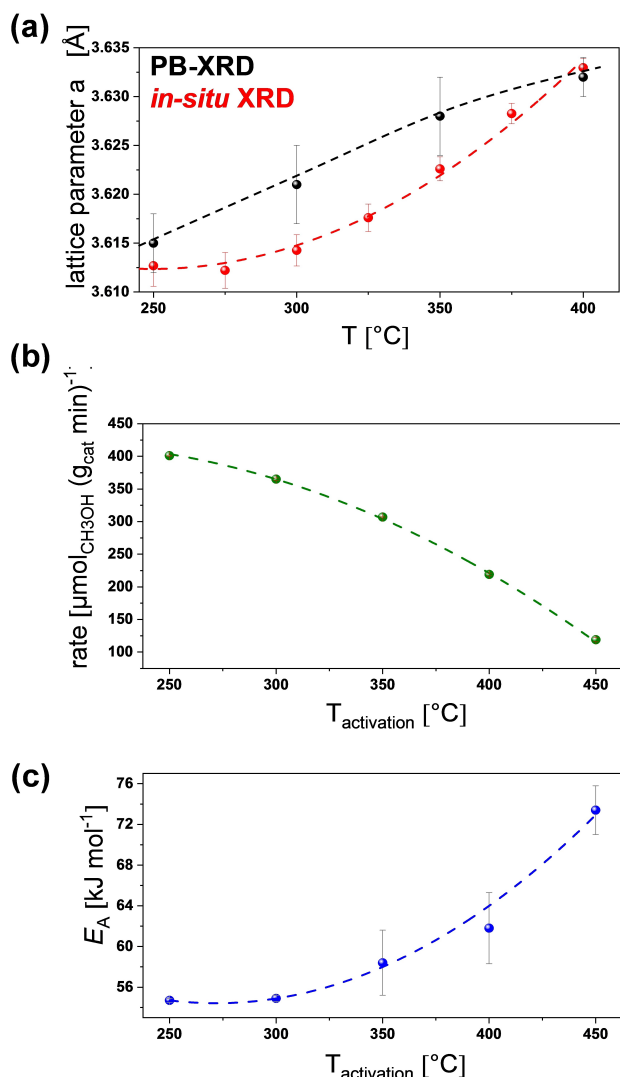


Figure 1. Lattice parameter of Cu plotted as a function of the activation temperature in a reductive atmosphere of 20% H₂ in He, measured by *in-situ* XRD (red) and *ex-situ* parallel beam (black) XRD (a). The CH₃OH reaction rates obtained from steady state measurements at 30 bar, 230 °C and synthesis gas (8CO₂/6CO/59H₂/27He) activated at various temperatures (b). Apparent activation energies at different activation temperatures at 30 bar in synthesis gas (c). The activation period prior to the measurements (b + c) were conducted in 20% H₂ in Ar and heating rates of 1 °C min⁻¹. All dashed lines are guides to the eye.

300 °C. These values, also with respect to the error bars (3 σ), are interpreted as signs of surface alloy formation already occurring at lower temperature. This is in line with the general process of Zn diffusion into the Cu lattice in reductive atmosphere starting at the surface.^[12] A comparison of the lattice parameter at 400 °C gives the identical results for BB and PB geometry evidencing an adaption of the surface and bulk values. The Zn concentration in CuZn-alloy (α -brass) is estimated as ~10 at.-%.^[13]

To correlate the starting alloy formation with the catalytic performance, Cu/ZnO:Al catalysts were activated at different temperatures and kinetically evaluated. The corresponding

reaction rates at 30 bar, 230 °C in syngas (8CO₂/6CO/59H₂/27He) are shown in Figure 1(b). With increasing activation temperature, the reaction rates of CH₃OH formation decrease. The loss in activity for the first increase in activation temperature (250 °C \rightarrow 300 °C; Δ rates = 41) is rather small and grows stepwise (300 °C \rightarrow 350 °C; Δ rates = 56/350 °C \rightarrow 400 °C; Δ rates = 88). This means that with ongoing alloy formation also the reaction rates to CH₃OH significantly decrease.

Since Cu and ZnO domain sizes (determined by Rietveld fitting of *in-situ* XRD data, Figure S2) grow continuously as a function of temperature, the contribution of a temperature induced decrease in reaction sites (due to e.g. sintering, domain size growth etc.) has to be evaluated. Figure 2 illustrates the specific surface areas of the differently activated catalysts determined by H₂-TPD and N₂O-RFC. This quantification allows discriminating between exclusively Cu-surface sites (H₂-TPD) and redox active sites on the surface (N₂O-RFC), which include additionally oxygen vacancies on ZnO and CuZn-alloy sites.^[14] The N₂O-RFC values decrease insignificantly (from 29.4 \rightarrow 27.5 m²g⁻¹) with increasing activation temperatures (from 250 \rightarrow 350 °C) and drop by more than one third upon reaching 400 °C. This implies that at elevated temperature alloy formation has already a significant influence on the overall specific surface area. The Cu surface area slightly increases (~1 m²g⁻¹) between 250 and 300 °C activation temperature and strongly decreases at 350 °C (to ~5 m²g⁻¹). This is explained by the limited ability of the CuZn-alloy, which is according to Figure 1(a) + (b) already present, to activate H₂. Since N₂O is able to react with Cu and Zn from the surface alloy, the N₂O-RFC values are almost unaffected (Figure 2). The increasing number of Cu sites between 250 and 300 °C is attributed to the crystallization of amorphous ZnO moieties, which partly cover the Cu surface by a metastable overlayer (Figure S3).^[7d] This is further confirmed by a quantitative analysis of the ZnO phase by PB-XRD, which shows an increasing ZnO-phase near the surface (Figure S4).

The significant amount of CuZn-alloy at an activation temperature of 350 °C is in line with the apparent activation energies (E_A) for CH₃OH formation shown in Figure 1(c). E_A starts

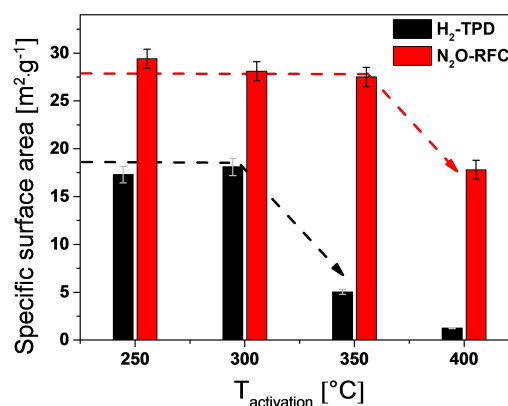


Figure 2. Specific surface area values of differently activated catalysts determined by H₂-TPD and N₂O-RFC.

to increase with increasing amount of CuZn-alloy (see also Figure S5). This means that the alloy formation negatively influences the nature of the active site. This trend continues, and with higher activation temperature higher E_A are obtained due to the increase in CuZn-alloy formation. E_A at 300 °C seems to be unaffected, which is explained by the non-stable character of surface alloy under industrially relevant testing conditions.^[7d,15] This indicates that significant amounts of H₂O are present and re-oxidize the Cu–Zn sites back to Cu–ZnO.^[6f,7b] This phenomenon is well-known and studied in the literature and precisely explains the almost stable specific surface area and E_A values. The slightly decreasing reaction rates (Figure 1b) are explained by the loss of the interfacial Cu–ZnO contact due to de-wetting and crystallization of the metastable ZnO-moieties (number of reaction sites influenced, not the nature).

To gain a deeper insight into the state of the samples after activation at 250 °C (no CuZn-alloy) and 350 °C (with CuZn-alloy), *in-situ* XAS measurements at the Cu and Zn K-edges were performed. The activation of a Cu/ZnO:Al catalyst itself is a complex process, involving HT-CO₃ decomposition, Cu reduction, ZnO polymorphism, self-doping and charge transfer. This intriguing interplay leads to the formation of an intimate interfacial Cu–ZnO contact and was subject of a separate, recently published study.^[9] Here, we focus on structural changes upon exceeding 250 °C under reductive atmosphere (5% H₂ in He). Figure 3(a) shows Zn K-edge XANES spectra of the Cu/ZnO:Al catalyst along with ZnO and Zn metal reference spectra. At RT the XANES spectrum looks very similar to the ZnO bulk reference sample with Zn in the oxidation state (II). The slightly broadened and weaker features in intensity evidence the nanostructured character of ZnO moieties within the CuO/ZnO:Al precatalyst. Heating the sample in reductive atmos-

phere leads to a decrease in whiteline intensity at 9669 eV, indicating a slightly reduced character of Zn (II-x). Between 250 °C and 350 °C, the differences in the Zn K-edge XANES spectra seem to be negligible, however, the corresponding derivative spectra shown in Figure 3(b) reveal further details: The decrease in the whiteline intensity and its shift towards lower energies at ~9662.5 eV (1s–4p transition) in the derivative spectra is interpreted as a change in the coordination environment of a small fraction of Zn²⁺ (octahedral→tetrahedral).^[9] This is coupled to an increase in covalence and loss of ionicity (ZnCO₃→ZnO), respectively, and stays stable up to 350 °C (complete decomposition of residual carbonate already at 250 °C). The Zn metal reference spectrum shows a characteristic maximum at 9658.5 eV. This spectral feature is absent in the precatalyst, but starts to grow gradually with increasing temperature (250 °C→350 °C). The increase at 9658.5 eV directly evidences the reduction of ZnO moieties and indicates the formation of small fractions of Zn⁰ as part of CuZn-alloy (see also Figure 1 and 2). As the reduction temperature is raised, Cu is reduced to Cu⁰ (Figure 3c, Cu K-edge spectra) and again only minor differences between spectra recorded at 250 and 350 °C are observed. The differences between the pre-edge features in the spectra of Cu metal and Cu/ZnO:Al are attributed to the presence of Cu nanostructures.^[7f,16] The corresponding Fourier transformed (FT) EXAFS data, in Figure 3(c) as inset, show a decrease in peak amplitude indicating a higher degree of structural disorder (see Debye-Waller factors in Table S2, and fitting curves in Figure S7) with increasing temperature. This behavior might be interpreted as the beginning of CuZn-alloy formation, but it more likely indicates a surface event without a α -brass or bulk contribution (here: $R=2.55$ Å vs. $R=2.66$ Å for CuZn alloy,^[7b] see also Table S2). To probe the stability of the CuZn-alloy, the temperature was increased to 400 °C and the gas atmosphere was switched to reverse water-gas shift (rWGS) conditions (1 bar, 10% H₂, 10% CO₂, 80% He, flow 50 ml·min⁻¹). The derivative Zn K-edge XANES spectra are compared in Figure 3(d). Even at high temperatures, where alloy formation is forced, the impact of the applied rWGS reaction conditions is unambiguous. The CuZn-alloy formation which occurred during reductive treatment, is reversible, and the alloy is re-oxidized by CO₂/H₂O under reaction conditions. This is also confirmed by the EXAFS fitting results summarized in Table S2, showing a constant coordination number of Cu coupled to an increase in structural disorder (250 °C: $N=8.7 \pm 1.4$; $\sigma^2=14.4 \pm 1.7 \cdot 10^{-3}$ Å²/400 °C: $N=8.7 \pm 1.9$; $\sigma^2=18.2 \pm 2.6 \cdot 10^{-3}$ Å²). Since the alloy formation depends on the H₂ concentration (5% H₂ at 400 °C), the *in-situ* XRD experiment was adapted for comparison (Figure S6). The results discussed in Figure 1, with respect to the amount of formed alloy and its reversible character under reaction conditions, are perfectly in line with the amount of alloy formed under 5% H₂ at 400 °C (Figure S5). As long as only a small fraction of CuZn-alloy (likely on the surface) is formed, it is re-oxidized to Cu–ZnO. As a consequence, the loss in catalytic activity is explained by the temperature induced sintering and phase segregation tendencies decreasing the number of active sites. Our group recently published a study highlighting the strong impact of H₂O under CH₃OH synthesis conditions.^[17]

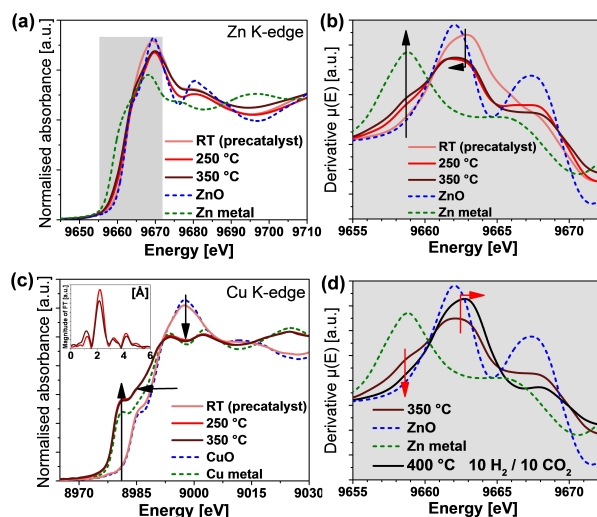


Figure 3. Zn K-edge XANES spectra of the Cu/ZnO:Al catalyst at various temperatures, ZnO and Zn references (a). Zn K-edge derivative XANES spectra (b). Cu K-edge spectra at various temperatures for the Cu/ZnO:Al catalyst, CuO and Cu metal references and Fourier transformed Cu K-edge EXAFS data (c). Derivative of the Zn K-edge spectra including data recorded under rWGS conditions at 400 °C (d). The heating is conducted in 5% H₂ in He.

Coverages of 1–2 monolayers of H₂O were identified as being present under industrially relevant conditions. As soon as a bulk alloy is formed (Figure 1, 400 °C in 20% H₂), the influence on the catalytic material seems to be partly irreversible (Figure 1b + c), at least under the applied conditions.

The origin of the CuZn alloy formation, as stepwise process controlled by the activation temperatures and the redox potential of the gas phase (minimizing the surface energy, ZnO reduction, Zn diffusion in Cu, α -brass formation),^[7f,18] is also locally visible by transmission electron microscopy (TEM, Figure 4, Figure S8). After reductive treatment at 350 °C the high resolution TEM image displays the presence of ZnO islands on top of a defective Cu-rich Cu₃Zn nanoalloy. Note that due to the similar lattice planes of metallic Cu and Cu₃Zn (Table S3) a direct phase assignment is not trivial. However, elemental mapping of the catalyst activated at 400 °C shows already a CuZn-nanoalloy particle embedded in ZnO, representing bulk-alloy moieties (Figure S8c, elemental mapping based on electron energy loss spectroscopy).

In summary, the activation of a Cu/ZnO:Al catalyst is a sensitive process. Exceeding 250 °C has already severe consequences for the catalytic performance and the involved active sites. Discussing the active site concept as interfacial site at the Cu–ZnO perimeter the catalytic adaptations are unraveled. Under defined reducing conditions (here, 20% H₂ in Ar) CuZn-alloy formation is enforced (early stage of α -brass). When approaching a certain amount of CuZn-alloy, the catalyst is irreversibly modified, which also leads to a change in the nature of the active site (removing oxygen at the perimeter of Cu–O–Zn). The decrease of the reaction rate coupled to an increase of the CuZn-alloy formation and E_A might be explained by the multiple synergisms focused at the in Cu–ZnO interface (structurally, electronically and mechanistically). A CuZn-alloy might be an

active structure for CH₃OH synthesis, but not all synergistic effects are observable (e.g. unable to activate H₂,^[14a] too stable oxygenates,^[6f] no OH-groups to activate CO₂-derived intermediates^[17]). Besides, the formation of a small fraction of CuZn-alloy (likely on the surface/interface of Cu–ZnO) is, under relevant conditions, structurally a reversible phenomenon (re-oxidation to Cu–O–Zn). Finally, this study identifies the lattice constant of Cu as descriptor of its specific activity, defined by the alloy formation during activation as unwanted state of the active site.

Acknowledgement

KIT's synchrotron radiation source (operated by KIT-IBPT) is acknowledged for providing beamtime at the CAT-ACT beamline, in particular Dr. Tim Pr ubmann and Dr. Anna Zimina (IKFT) for their help and technical support during XAS experiments. We thank the BMBF for funding the project "MatAct" (05K10VKB) to support operando catalysis infrastructure at ANKA. Prof. Jan-Dierk Grunwaldt, KIT Institute for Chemical Technology and Polymer Chemistry and Institute of Catalysis Research and Technology, is greatly acknowledged for his support and fruitful discussions.

Conflict of Interest

The authors declare no conflict of interest.

Keywords: methanol synthesis · CuZn-alloy formation · Cu lattice parameter · Cu/ZnO-interface · In-situ XAS/XRD

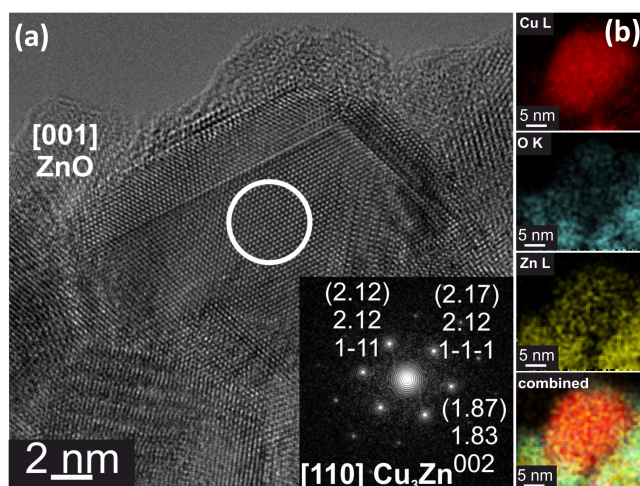


Figure 4. (a) TEM image after reductive activation at 350 °C. The circle denotes the region from which the Fast Fourier Transform (FFT) was acquired. The inset displays the corresponding FFT. The distances in the FFT are given in [Å]. (b) Elemental EELS mapping of Cu L-, O K-, and Zn L-edges after reductive activation at 400 °C. The Cu/ZnO:Al catalysts were activated in 20% H₂ in Ar and transferred without contact to ambient into the microscope.

- [1] F. Haber, *J. Soc. Chem. Ind.* **1914**, 33, 49–54.
- [2] a) H. S. Taylor, *Proc. Roy. Soc. London Ser. A* **1925**, 108, 105–111; b) F. H. Constable, *Math. Proc. Cambridge Philos. Soc.* **1926**, 23, 172–182; c) I. Langmuir, *J. Am. Chem. Soc.* **1918**, 40, 1361–1403; d) A. F. Benton, *J. Am. Chem. Soc.* **1923**, 45, 887–899; e) R. N. Pease, *J. Am. Chem. Soc.* **1923**, 45, 1196–1210.
- [3] G. A. Somorjai, K. R. McCrea, J. Zhu, *Top. Catal.* **2002**, 18, 157–166.
- [4] M. Hävecker, S. Wrabetz, J. Kröhnert, L.-I. Csepei, R. Naumann d'Alnoncourt, Y. V. Kolen'ko, F. Girgsdies, R. Schlögl, A. Trunschke, *J. Catal.* **2012**, 285, 48–60.
- [5] R. Schlögl, *Angew. Chem. Int. Ed.* **2015**, 54, 3465–3520; *Angew. Chem.* **2015**, 127, 3531–3589.
- [6] a) K. Klier, in *Adv. Catal.*, Vol. 31 (Eds.: D. D. Eley, H. Pines, P. B. Weisz), Academic Press, **1982**, pp. 243–313; b) R. Burch, S. E. Golunski, M. S. Spencer, *J. Chem. Soc. Faraday Trans.* **1990**, 86, 2683–2691; c) J. Nakamura, T. Uchijima, Y. Kanai, T. Fujitani, *Catal. Today* **1996**, 28, 223–230; d) I. Kasatkin, P. Kurr, B. Kniep, A. Trunschke, R. Schlögl, *Angew. Chem.* **2007**, 119, 7465–7468; *Angew. Chem. Int. Ed.* **2007**, 46, 7324–7327; e) M. Behrens, F. Studt, I. Kasatkin, S. Kühl, M. Hävecker, F. Abild-Pedersen, S. Zander, F. Girgsdies, P. Kurr, B.-L. Kniep, M. Tovar, R. W. Fischer, J. K. Nørskov, R. Schlögl, *Science* **2012**, 336, 893–897; f) S. Kattel, P. J. Ramirez, J. G. Chen, J. A. Rodriguez, P. Liu, *Science* **2017**, 355, 1296–1299; g) S. Kuld, M. Thorhaug, H. Falsig, C. F. Elkjær, S. Helveg, I. Chorkendorff, J. Sehested, *Science* **2016**, 352, 969–974; h) K. C. Waugh, *Catal. Today* **1992**, 15, 51–75.
- [7] a) P. L. Hansen, J. B. Wagner, S. Helveg, J. R. Rostrup-Nielsen, B. S. Clausen, H. Topsøe, *Science* **2002**, 295, 2053–2055; b) J.-D. Grunwaldt, A. M. Molenbroek, N. Y. Topsøe, H. Topsøe, B. S. Clausen, *J. Catal.* **2000**, 194, 452–460; c) F. Studt, M. Behrens, E. L. Kunkes, N. Thomas, S. Zander, A. Tarasov, J. Schumann, E. Frei, J. B. Varley, F. Abild-Pedersen, J. K. Nørskov, R. Schlögl, *ChemCatChem* **2015**, 7, 1105–1111; d) T. Lunken-

- bein, F. Girgsdies, T. Kandemir, N. Thomas, M. Behrens, R. Schlögl, E. Frei, *Angew. Chem.* **2016**, *128*, 12900–12904; *Angew. Chem. Int. Ed.* **2016**, *55*, 12708–12712; e) O. Martin, J. Pérez-Ramírez, *Catal. Sci. Technol.* **2013**, *3*, 3343–3352; f) D. Grandjean, V. Pelipenko, E. D. Batyrev, J. C. van den Heuvel, A. A. Khassin, T. M. Yurieva, B. M. Weckhuysen, *J. Phys. Chem. C* **2011**, *115*, 20175–20191; g) C. V. Ovesen, B. S. Clausen, J. Schiøtz, P. Stoltze, H. Topsøe, J. K. Nørskov, *J. Catal.* **1997**, *168*, 133–142.
- [8] a) J. Schumann, J. Kröhnert, E. Frei, R. Schlögl, A. Trunschke, *Top. Catal.* **2017**, *60*, 1735–1743; b) C. Tisseraud, C. Comminges, S. Pronier, Y. Pouilloux, A. Le Valant, *J. Catal.* **2016**, *343*, 106–114; c) C. Álvarez Galván, J. Schumann, M. Behrens, J. L. G. Fierro, R. Schlögl, E. Frei, *Appl. Catal. B* **2016**, *195*, 104–111; d) S. D. Senanayake, P. J. Ramírez, I. Waluyo, S. Kundu, K. Mudiyansele, Z. Liu, Z. Liu, S. Axnanda, D. J. Stacchiola, J. Evans, J. A. Rodríguez, *J. Phys. Chem. C* **2016**, *120*, 1778–1784; e) J. Schumann, M. Eichelbaum, T. Lunkenbein, N. Thomas, M. C. Álvarez Galván, R. Schlögl, M. Behrens, *ACS Catal.* **2015**, *5*, 3260–3270.
- [9] E. Frei, A. Gaur, H. Lichtenberg, C. Heine, M. Friedrich, M. Greiner, T. Lunkenbein, J.-D. Grunwaldt, R. Schlögl, *ChemCatChem* **2019**, *11*, 1587–1592.
- [10] J. Schumann, T. Lunkenbein, A. Tarasov, N. Thomas, R. Schlögl, M. Behrens, *ChemCatChem* **2014**, *6*, 2889–2897.
- [11] a) R. W. Cahn, *Adv. Mater.* **1991**, *3*, 628–629; b) J. P. Neumann, T. Zhong, Y. A. Chang, *Bull. Alloy Phase Diagrams* **1984**, *5*, 136–140; c) P. B. Lloyd, J. W. Kress, B. J. Tatarchuk, *Appl. Surf. Sci.* **1997**, *119*, 275–287.
- [12] M. S. Spencer, *Surf. Sci.* **1987**, *192*, 329–335.
- [13] a) T. Fujitani, J. Nakamura, *Catal. Lett.* **1998**, *56*, 119–124; b) K.-D. Jung, O.-S. Joo, S.-H. Han, *Catal. Lett.* **2000**, *68*, 49; c) S. S. R. a. T. R. Anantharaman, *Curr. Sci.* **1963**, *32*, 262.
- [14] a) S. Kuld, C. Conradsen, P. G. Moses, I. Chorkendorff, J. Sehested, *Angew. Chem. Int. Ed.* **2014**; b) M. B. Fichtl, J. Schumann, I. Kasatkin, N. Jacobsen, M. Behrens, R. Schlögl, M. Muhler, O. Hinrichsen, *Angew. Chem. Int. Ed.* **2014**, *53*, 7043–7047; *Angew. Chem.* **2014**, *126*, 7163–7167.
- [15] G. C. Chinchin, K. C. Waugh, D. A. Whan, *Appl. Catal.* **1986**, *25*, 101–107.
- [16] L. S. Kau, K. O. Hodgson, E. I. Solomon, *J. Am. Chem. Soc.* **1989**, *111*, 7103–7109.
- [17] A. V. Tarasov, F. Seitz, R. Schlögl, E. Frei, *ACS Catal.* **2019**, *9*, 5537–5544.
- [18] M. S. Spencer, *Surf. Sci.* **1987**, *192*, 323–328.

Manuscript received: May 7, 2020

Revised manuscript received: May 12, 2020

Accepted manuscript online: May 12, 2020

Version of record online: June 18, 2020